Paper number 14-3035

DEVELOPMENT OF A COMPUTATIONAL APPROACH TO DETECT INSTABILITY AND INCIPIENT MOTION OF LARGE RIPRAP ROCKS

Cezary BOJANOWSKI – corresponding author
Transportation Research and Analysis Computing Center (TRACC),
Energy Systems Division
Argonne National Laboratory
9700 S. Cass Ave, Building 222
Argonne, IL 60439, USA
Phone: 1-630-252-5294; Fax: 1-630-252-5461; E-mail: cbojanowski@anl.gov

Steven LOTTES
Transportation Research and Analysis Computing Center (TRACC),
Energy Systems Division
Argonne National Laboratory
9700 S. Cass Ave, Building 222
Argonne, IL 60439, USA
Phone: 1-630-252-5290; Fax: 1-630-252-5461; E-mail: slottes@anl.gov

ABSTRACT
Computational fluid dynamics (CFD) has progressed to the point where flow problems can be solved in domains containing solid objects with complex, irregular geometry in relative motion along arbitrary paths through the fluid domain. The solvers incorporate moving mesh and mesh morphing techniques. With this new CFD capability the detailed stress distribution created by flow over the surface of a moving solid and the capability of computational structural mechanics (CSM) software to solve for both small and large displacements of solids from applied loads, it is now possible to solve a wide variety of fluid structure interaction (FSI) problems by coupling the two types of software. This paper presents development of procedures to couple STAR-CCM+® CFD software to LS-DYNA® CSM software to solve FSI problems. An initial application of the coupled software to FSI analysis of incipient motion of large riprap rocks is described. Two cases were used to test the coupling. The first has a rock layer in a channel with no bridge structures, and the second has an abutment corner that contracts the flow. Three representative rocks were included in the coupling and the approximate inlet flow velocity required to lift a rock and move it downstream was determined.

Keywords: FSI, riprap, incipient motion, critical velocity

1 INTRODUCTION

The sizing of riprap in scour countermeasure design procedures is based mostly on limited field observations and scaled laboratory tests under ideal, controlled conditions. The size of riprap required for many field applications is too large for testing in the laboratory. As a consequence there is significant uncertainty in the formulas for sizing riprap. For example, as shown in Figure 1, there is a large spread in the design mean diameters, d_{50}, from formulas that have been proposed between 1973 and 1999 for piers. Most of these yield larger values than the current HEC-23 formula *(1)*, which is functionally equivalent to the 1936 Isbash formula with an added K factor applied to the mean velocity that is meant to account for the higher instantaneous velocities around different pier shapes that are a function of the turbulence intensity. Recent advances in the capabilities of both computational fluid dynamics (CFD) and computational structural mechanics (CSM) software have made it possible to analyze the onset of rock motion in riprap based on a highly detailed pressure distribution acting on the surface of rocks, and to extend this to tracking the subsequent motion of individual rocks and their interaction with other rocks or the solid surfaces of a pier or abutment. This paper describes the development of a coupling process between CFD and CSM software that provides the capability to carry out this type of analysis and includes two examples that demonstrate the capabilities needed for the analysis.

Fluid structure interaction (FSI) problems involve solving for the fluid flow force load on a solid surface and the response of the solid to the load. In recent years a number of CFD and CSM software vendors have been developing the capabilities needed to solve FSI problems. In many cases these vendors are recognized leaders in the field of either CFD or CSM, but not both, and integrated FSI software, if available, is not yet mature and well tested by industry. Until industry proven FSI solvers are available, coupling highly robust and reliable CFD and CSM software through the development of data exchange and concurrent control coupling procedures appears to be the best approach to solving FSI problems. TRACC has licenses, a user base, and in house expertise in the use of the software for CD-adapco's STAR-CCM+ CFD software and LSTC's LS-DYNA CSM software. For this reason, these software packages were chosen to develop coupling procedures for the detailed analysis of the onset of motion of riprap rocks. CD-adapco was contacted regarding the feasibility of coupling and provided a list of the basic steps needed in the data exchange to couple STAR-CCM+ with CSM software.

NCHRP report 568 *(2)* lists four major failure modes for riprap revetments including (i) slope failure resulting in a slide, (ii) riprap particle erosion due to undersized riprap, (iii) erosion beneath the armoring layers of riprap, and (iv) erosion of the toe or key of the revetment leading to a slide failure. In the method developed here, detailed computation of riprap rock motion using FSI techniques can be applied to analysis of failure modes (i), (ii), and (iv). A scour model capable of handling scour beneath a riprap revetment would be required to analyze failure mode (iii). The FSI methods developed for analysis of conditions that lead to riprap failure rely on knowing the detailed bathymetry of the riverbed, geometry of structures and of the irregular surface of the armor layer. Ideally, a complete mapping of the irregular geometry of the armor layer would be available for construction of the computational mesh, however, sufficient engineering accuracy may be obtained with a reasonable approximation of the armor bed geometry. In this initial effort, the motion of just a few representative rocks at the surface of the armor layer is computed. The Turner-Fairbank Laboratory *(3)* provided cloud point scans of the irregular surface representative rocks for the analysis. MeshLab software *(4)* was used to process the point scans to obtain the surface geometry of a rock. Several rocks with different shapes were used in the computations based on the modifications of the geometry of the scanned rock. Most of the effort in developing the FSI coupling went into resolving moving and morphing mesh problems that arise when rock motion collapses the space between a rock and another solid surface and problems that arose in the mapping and data exchange between the CFD and CSM software. The resolution of these problems yielded coupling software for data mapping, data exchange, and automated mesh morphing failure recovery that make it possible to carry out the analysis. The functioning of automated procedures is demonstrated in computation of water flow at increasing velocities until rock motion into the downstream occurs. A riverbed geometry with no obstructions and a geometry with an abutment corner are analyzed to illustrate the method.

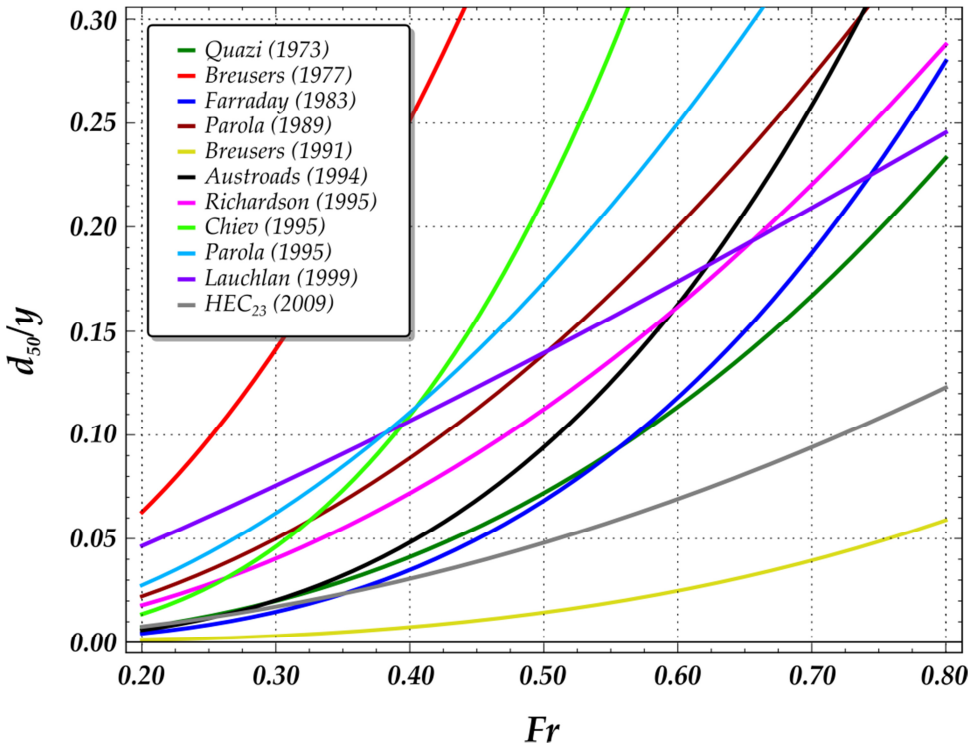

FIGURE 1 Comparison of riprap sizing curves at a rectangular pier based on *(2)*.

2 COUPLING METHODOLOGIES FOR SOLVING FSI PROBLEMS

2.1 Governing Equations for the Fluid and Structural Domains

While there has been an interest in solving FSI problems for decades, large computer clusters capable of solving them for full scale systems have only become widely available in the past decade. In addition, moving and morphing mesh capabilities in CFD software needed to solve FSI problems have only recently matured to the point where they can be reliably used. This maturity was necessary before the coupling of CFD and CSM software could be expected to be successful.

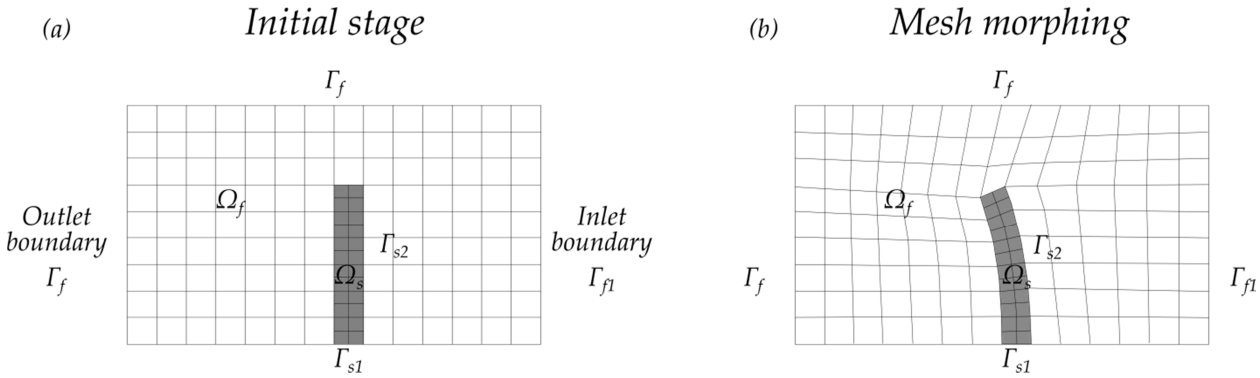

FIGURE 2 Initial stage of the FSI problem and an intermediate stage with mesh morphing.

Figure 2a presents a schematic of a discretized computational domain with fluid occupying space Ω_f and solid body occupying space Ω_s. The Reynolds averaged Navier-Stokes (RANS) equations for Newtonian incompressible fluids were used with a k-ε turbulence model to solve for the flow field and pressure distribution on the rock surfaces. The conservation of momentum and mass equations represented by RANS equations are *(5)*:

$$\rho\left(\frac{\partial u_i}{\partial t}+\left(u_j-v_j\right)\frac{\partial u_i}{\partial x_j}\right)=-\frac{\partial p}{\partial x_i}+\frac{\partial}{\partial x_i}\left(\mu_{eff}\frac{\partial u_i}{\partial x_j}\right)+\rho g_i \qquad in \qquad \Omega_f \tag{1}$$

$$\frac{\partial(u_i-v_i)}{\partial x_i}=0 \qquad in \qquad \Omega_f \tag{2}$$

where ρ is the fluid density, u_i is the Reynolds averaged velocity in the i-direction, v_j is the mesh velocity in the j-direction, p is the pressure, $\mu_{eff} = \mu + \mu_t$ is the effective viscosity, $\mu_t = \rho\, C_\mu\, k^2/\varepsilon$ is the turbulent viscosity, and g_i is the i-direction component of the gravity vector. The standard equations for turbulent kinetic energy, k, and dissipation rate, ε, are given by:

$$\rho\left(\frac{\partial k}{\partial t}+\left(u_j-v_j\right)\frac{\partial k}{\partial x_j}\right)=-\frac{\partial p}{\partial x_i}+\frac{\partial}{\partial x_i}\left(\left(\mu+\frac{\mu_t}{\sigma_k}\right)\frac{\partial k}{\partial x_j}\right)-\rho\varepsilon+\mu_t S^2 \qquad in \qquad \Omega_f \tag{3}$$

$$\rho\left(\frac{\partial \varepsilon}{\partial t}+\left(u_j-v_j\right)\frac{\partial \varepsilon}{\partial x_j}\right)=-\frac{\partial p}{\partial x_i}+\frac{\partial}{\partial x_i}\left(\left(\mu+\frac{\mu_t}{\sigma_\varepsilon}\right)\frac{\partial \varepsilon}{\partial x_j}\right)+C_{1\varepsilon}\frac{\varepsilon}{k}\mu_t S^2-C_{2\varepsilon}\rho\frac{\varepsilon^2}{k} \qquad in \qquad \Omega_f \tag{4}$$

where $S = (2\, S_{ij}\, S_{ij})^{1/2}$ is the norm of the mean strain rate tensor of the fluid, and the model constants are $C_\mu = 0.09$, $\sigma_k = 1.0$, $\sigma_\varepsilon = 1.3$, $C_{1\varepsilon} = 1.44$, and $C_{2\varepsilon} = 1.92$. STAR-CCM+ contains options to select a wide variety of variations of RANS turbulence models. To better handle the geometry variations in the domain, the more general realizable k-ε model with a blended wall function formulation to determine shear stress at solid boundaries was used for this work. Details can be found in the user guide *(5)*. The initial and boundary conditions for the fluid domain are:

$$\xi\big|_0 = \xi^0 \qquad in \qquad \Omega_f(0) \tag{5}$$

$$\xi = \xi_b \qquad on \qquad \Gamma_{f1} \tag{6}$$

$$\frac{\partial \xi}{\partial n} = h_b \qquad on \qquad \Gamma_{f2} \tag{7}$$

where $\xi \in \{u_x, u_y, u_z, p, k, \varepsilon\}$ and ξ_b and h_b are known boundary values for Dirchlet, Γ_{f1}, and Neuman, Γ_{f2}, boundary conditions respectively. Information on setting consistent boundary values for inlet, outlet, pressure, wall, and symmetric boundaries is contained in the user guide *(5)*. The solid part of the domain Ω_s is governed by the following conservation equations (see references *(6)* and *(7)* for details):

$$\rho\frac{\partial u_i}{\partial t}=\frac{\partial \sigma_{ij}}{\partial x_j}+\rho g_i \qquad in \qquad \Omega_s \tag{8}$$

$$\sigma_{ij} n_i = t_i \qquad on \qquad \Gamma_{s1} \tag{9}$$

$$x_i\big|_0 = x_i^0 \qquad on \qquad \Gamma_{s2} \tag{10}$$

$$\left(\sigma_{ij}^+ - \sigma_{ij}^-\right)n_i = 0 \qquad on \qquad \Gamma_{s3} \tag{11}$$

where σ_{ij} are components of the stress tensor, n_i are the components of the surface normal vector, t_i are components of external surface forces, and equation 11 requires equality of contact forces at the interface of two solids in contact.

In most classical CFD problems the boundaries are fixed during the analysis, and the computational mesh does not change. Notable exceptions are turbo machinery and in-cylinder combustion simulation where special techniques were developed to handle the moving boundaries. In FSI problems the fluid boundaries may be part of a structure that will move or deform in response to surface and body forces that are determined as part of the solution of the problem. As the boundary motion is calculated, the computational mesh in the fluid domain has to be updated either by a morphing procedure or a complete domain remesh process. The coupling conditions on the interface between the fluid and solid domains of an FSI problem are:

$$u_f = u_s \qquad on \qquad \Gamma_f = \Gamma_s \tag{12}$$

$$n \cdot \sigma_f = n \cdot \sigma_s \qquad on \qquad \Gamma_f = \Gamma_s \tag{13}$$

where σ_f and σ_s are the fluid and solid side stress tensors respectively.

The CFD solution of the fluid flow equations yields the detailed distribution of fluid stress on solid surfaces (left hand side of equation 13). This stress distribution is passed to the CSM software to solve for the response of the solid bodies, and that solution yields the displacement rate (velocity) distribution of the solid surfaces (right hand side of equation 12). In general, the surface velocity distribution may include both deformation and rigid body motion. In the analysis of riprap rock motion, it includes only rigid body motion. The motion computed by the CSM software is passed to the CFD software as a boundary condition that is a function of time.

2.2 Methodologies of Coupling Codes

In general there are two groups of coupling solutions for FSI problems: monolithic and partitioned *(8)*. The monolithic approach involves solving the coupled set of equations for the fluid and structural domain as a single problem. Although this approach may seem the most natural one, it can be more difficult to adjust solver parameters to obtain a converged solution than with the partitioned approach. The use of robust CFD and CSM software from vendors who specialize in those areas naturally leads to using a partitioned approach where the equations are solved iteratively one domain at a time and coupling conditions are set via file based data exchange from the solution of the other domain.

Depending on the magnitude of the influence of interface boundary condition changes computed in either the solid or fluid domain on the other domain one-way or two-way coupling may be needed to solve the problem. If, for example, displacements of the structure due to fluid forces are small enough so that they do not substantially influence the fluid flow, then one way coupling from the fluid domain to the structural domain can be used. In this case the pressure distribution on the structure is not affected much by its motion, and therefore flow equations need to be solved only once to obtain the load from the flow on the structure. In rip-rap FSI analysis the motion of a rock results in an evolving position and orientation that substantially changes the pressure distribution over the surface of the rock, requiring two-way coupling for this problem.

Two way coupling can be either weak or strong. Weak coupling is presented in Figure 3a. In a loosely coupled step *n,* the solution in the fluid region, a pressure field, is found on the position of the boundaries at the start of the time step obtained from the structural solver from the previous step *n-1*. This pressure field is subsequently passed to the structural solver, which will yield a solution giving the solid boundary displacement and velocity that is passed to the CFD solver for use in time step *n+1*. The structural solver may require smaller time steps than the fluid solver if effects like contact, such as a rock colliding with surrounding rocks on the bed, are taken into account. Thus the fluid solver time step may be different than structural solver time step, however, the sum of time steps computed on both the structural and fluid domains between data exchange must be equal and that sum is the coupling time step. The number of steps and length of time steps is determined by the complexity of the physics modeled in each solver.

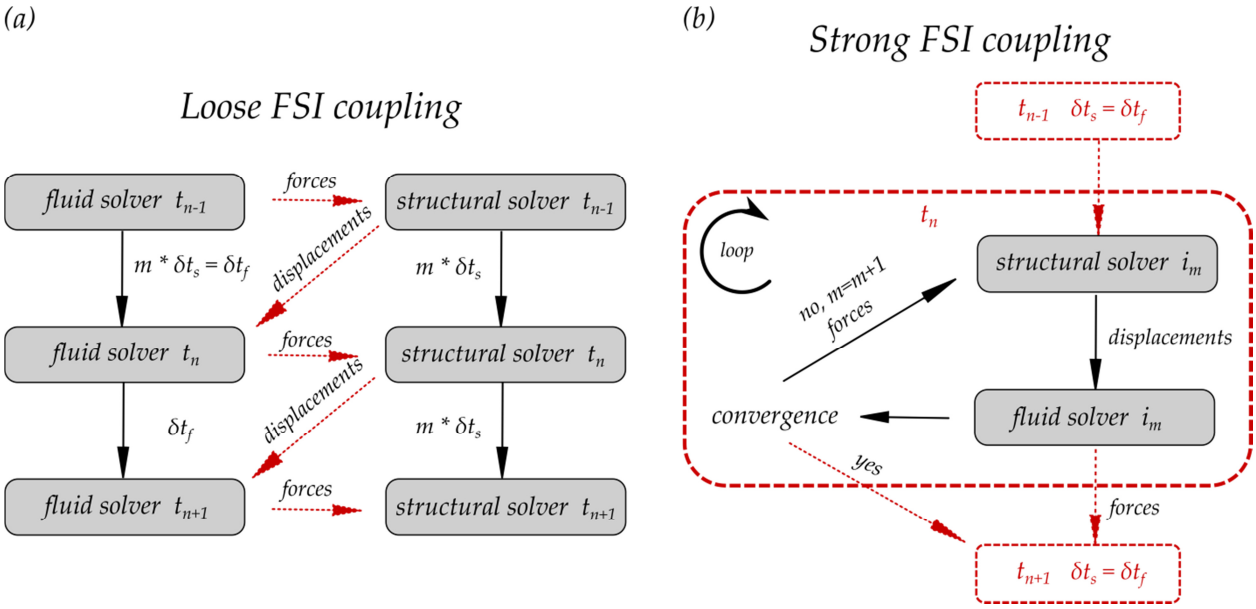

FIGURE 3 Loose and strong FSI coupling schemes.

Figure 3b presents a schematic of the strong coupling procedure. In this scheme the two problems are also numerically decoupled. However, within each time step *n*, the CFD and CSM solvers exchange interface conditions computed by the separate solvers during the iteration to converge the time step.

2.3 Workflow of the Current Implementation of File Based Data Exchange with Loose Coupling

The currently implemented loose coupling involves two separate solvers: STAR-CCM+ *(5)* performing CFD calculations and LS-DYNA *(6)*, *(9)* performing structural analysis. Both of these software packages have some FSI capabilities. However, LS-DYNA does not yet have sufficiently robust fluid flow solvers and the wide range of flow physics models available in STAR-CCM+, and STAR-CCM+ does not yet have the capability to handle contact forces between the objects that have a meshed geometry. A variety of models for particle-particle and particle-wall interactions exist, but those are sub-grid models of particles not represented in the mesh. For the purpose of analyzing the onset of motion of riprap rocks, modeling the effects of contact forces between objects represented in the mesh is an essential feature. For these reasons the analysis is split into two sub problems. STAR-CCM+ calculates the flow field and the pressure distribution on rocks, while LS-DYNA calculates the motion of rocks due to the stresses exerted by the fluid on the rock surface and the effects of contact forces. A new position of a rock after the coupling step is subsequently imported into STAR-CCM+ as a basis for the next time step calculation. Because the rocks are treated as rigid bodies, a loose coupling procedure that does not account for the acceleration of the rock during the time step is sufficient to obtain first order accuracy in the solution of the rock motion. The small time step required in LS-DYNA to handle body interactions and in STAR-CCM+ to keep the mesh morphing stable was assumed to be sufficient to compute the onset of rock motion and the trajectory to adequate engineering accuracy.

Figure 4 presents the workflow of the procedure to analyze incipient motion of riprap for a given arrangement and flow velocity. The procedure is executed in a LINUX environment with a control program written in the Python language. The program starts execution of needed components of LS-DYNA and STAR-CCM+, including the solvers and meshing software, and LS-PREPOST (LS-DYNA pre- and post-processing software). It also translates output files into a neutral NASTRAN format recognized by both software packages.

The analysis procedure begins with initialization runs in both solvers started manually. The LS-DYNA run provides the initial position of the rocks under gravity loading. This position is used as a basis

for CFD domain geometry. The CFD model is run until pseudo steady state conditions are achieved with all rocks stationary. Subsequently the Python program is started. Execution of the CFD part is quite complex and requires an internal Java macro to run within STAR-CCM+ to import rock displacements and map them from the CSM mesh to the CFD mesh and vice versa. It is almost always the case that the resolution between the fluid and structural grids is different, especially when two separate solvers are handling the fluid and solid domains. STAR-CCM+ provides accurate data mappers for non-conforming meshes *(5)*. This mapping has to be performed at each time step as the underlying mesh deforms. The effect of mesh morphing as a consequence of body motion is presented in Figure 2b. The displacements of the body are distributed throughout the morphed fluid domain to maintain cell quality. No cells are added or removed in the morphing process and their neighbor relationships are preserved so the mesh topology remains constant. The Arbitrary Lagrangian-Eulerian (ALE) algorithm is invoked to solve transport equations resulting from the moving underlying mesh *(5, 9)*. It allows for retaining the exact shape of the interface between the solid and the fluid.

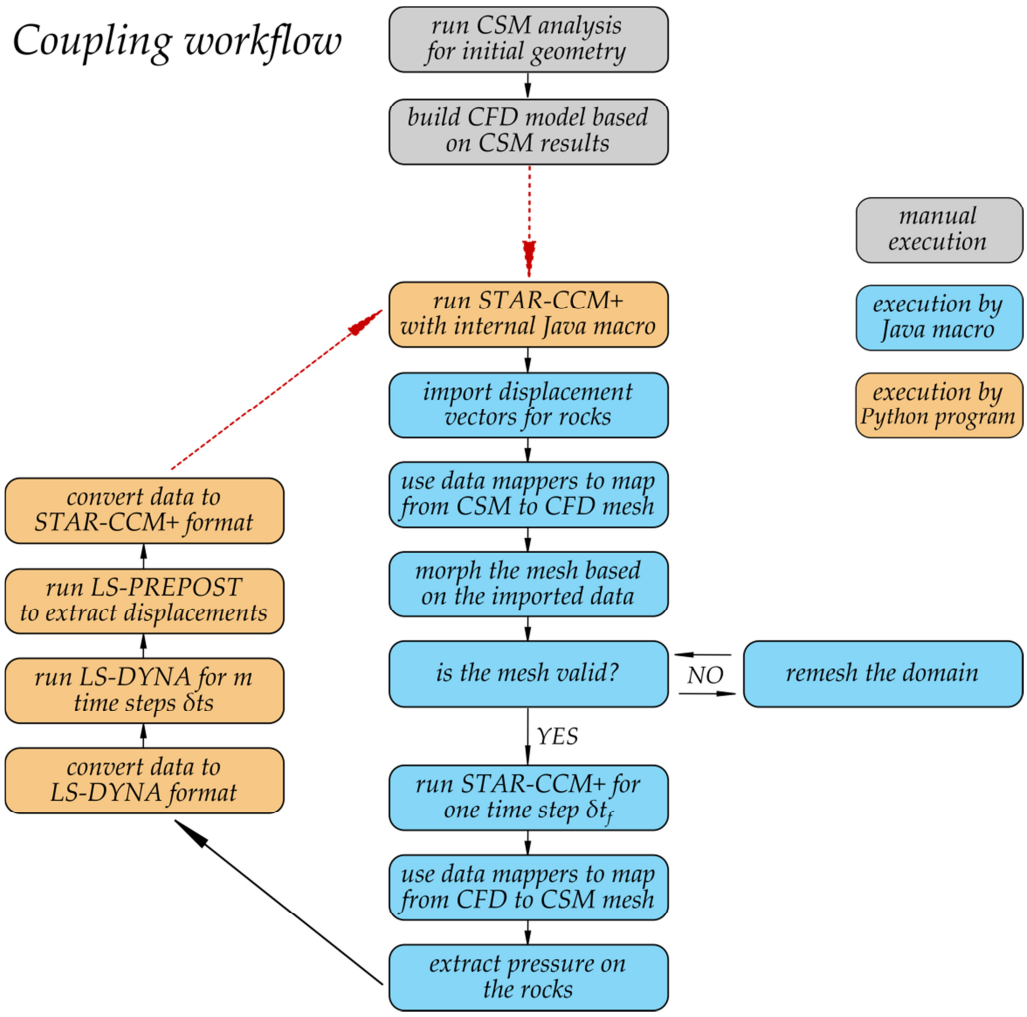

FIGURE 4 Current implementation of coupling workflow between STAR-CCM+ and LS-DYNA.

The mesh morpher uses a sophisticated algorithm that yields a high quality mesh in the whole computational domain based on the initial mesh and the displacement of the boundaries. However, in cases where the displacement of a rock becomes large or it comes in contact with a solid boundary, the cells may become too distorted and of such poor quality that the solver either diverges or encounters a floating point exception condition. In such cases the Java macro executes a computationally demanding

remeshing of the whole domain. The time step of calculations is selected such that full domain remeshing is avoided in the initial steps.

Once a CFD time step δt_f is converged, the pressure is mapped from the CFD mesh on the rocks to the CSM mesh and exported to file. The Java macro as well as the STAR-CCM+ solver are stopped. Next an LS-DYNA simulation is performed for m shorter time steps, δt_s, such that $m\ \delta t_s = \delta t_f$, the length of the coupling step. The resulting displacement vectors from LS-DYNA are extracted and translated to NASTRAN format so that they can be imported into STAR-CCM+ for the next step. After this the whole loop is repeated until the termination time.

2.4 Limitations of Current Implementation and Upcoming Developments

Using commercial software, as opposed to research software, has many advantages, the primary one being a large industrial user base engaged in using it successfully to solve problems on a daily basis, and consequently computed results are very reliable within the accuracy of the physics models used. Vendors responding to the needs of industry also implement a wide array of physics models, methods to solve a variety of moving mesh problems, and advanced solver algorithms. They normally provide a means for users to add new physics models in the form of user defined subroutines or functions. As such, they provide an excellent foundation for building models to solve new problems, or analyze classic problems using advanced analysis techniques. One disadvantage of using commercial software is that the users do not normally have direct access to the source code and therefore cannot make even minor modifications outside of the means provided by the vendor that might be needed for a new model development. That confines the user to the set of models and tools developed solely by the code owner that can be used when solving an engineering problem. The current implementation of coupling between STAR-CCM+ and LS-DYNA allows for capturing the main effects of rock motion, however, when domain remeshing occurs some of the information about the motion of a rock from step *n-1* to step *n* is lost, and the grid fluxes are not included in the momentum equations immediately after remeshing. As a result, the reduction in drag due to acceleration of a rock is not fully accounted for, and rock motion with large displacements will occur at a slightly lower velocity difference between the rock and mean flow. The error in this case is conservative in the sense that it would lead to slightly oversizing the riprap for a particular application.

3 APPLICATION OF THE METHOD TO RIPRAP STABILITY ANALYSIS

3.1 Model Development

The coupling procedures described in this paper were developed primarily for the purpose of applying them to the analysis of incipient motion of rocks used in riprap around piers or abutments to prevent scour of the riverbed at these structures. Initially, however, a very simple flat bed geometry with only riprap rocks present was used as a development base until all of coupling problems were resolved. This simple case also allowed for comparison with Laursen's and Neill's equations for critical velocities *(10)*.

Model development was started by processing the surface point cloud data from a 3D laser scan of a rock with ~4 mm spacing between the points provided by researchers at the Turner-Fairbank Highway Research Center *(3)*. MeshLab *(4)* software was used to generate a surface triangulation of the rock from the point cloud data (see Figure 5). The initial shape was subsequently modified by simple geometrical operations to create a set of rocks with similar shapes to populate the domain with rocks for testing. Several different rock shapes were used to create the configurations shown in Figure 6. Two layouts were considered in this analysis, layout 1, plain, Figure 6b, and layout 2, with abutment, Figure 6c. The grey rocks in the figures represent stationary rocks; these cannot move in the simulations as the FSI coupling was not activated for them. The three colored rocks in Figure 6b labeled rock 1, rock 2, and rock 3 can move and interact with other boundaries and among themselves through contact algorithms enabled in LS-DYNA. Rock 1 and rock 2 have exactly the same shape as the originally scanned rock in Figure 5. Rock 3 is bigger and more round than the other two but its longest internal measurement is the same, approximately 0.2 m (8 in). Rock 1 is placed flush with the other rocks in the bed. Rock 2 is placed quite deep under the top surface. Rock 3 is sticking out slightly above the bed. The shape of the rocks and their layout influences when they will be picked up and moved by the flow. Placing the rocks at different

locations ensures that each of them will have a different critical velocity determined by the detailed geometry and flow field computed in the simulation.

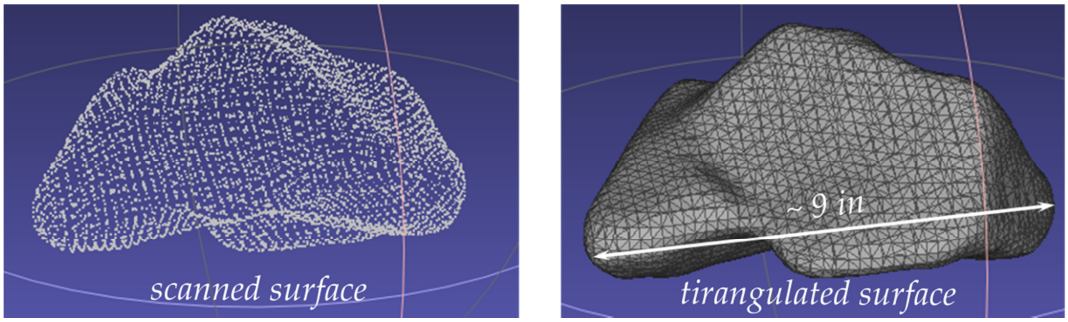

FIGURE 5 Point cloud of a scanned rock and its triangulated representation.

A CFD domain was built with dimensions: 5.0 m long, 1.2 m wide, and 0.65 m high in the recessed area containing the rocks of the riprap layer. The height of the water from the top to the riprap bed top surface was approximately 0.35 m. The size of the domain was designed to be small to conserve computational resources and provide fast turnaround times during development and testing of the coupling procedures. A single phase rigid lid model of the channel flow was also used to keep the model as simple and fast running as possible.

The right end of the domain was set as velocity inlet. The initial water velocity in the domain and the velocity at the inlet was a variable parameter that was manually changed from 2.0 to 3.0 m /s in 0.5 m/s intervals. The sides of the domain were set as symmetry planes. The right side of the model was set as an outflow boundary. In layout 2, with the abutment, the abutment is a wall boundary and the approach flow boundary on the abutment side of the domain was also set as wall boundary. The opposite side is set as a symmetry plane. The domain was meshed using hexahedral cells with varying cell size from 0.004 m (0.16 in) around the rocks up to 0.06 m (2.4 in) away from the rocks and other boundaries. The total count of cells in the model varied between 1.5 million up to 2.0 million cells depending on the layout (plain or abutment) and the evolving position of rocks during the simulation. A k-ε turbulence model with Reynolds-Averaged Navier Stokes equations was used to solve for the flow field. An implicit unsteady solver with time step of 0.01 sec was used in the flow solver. That was also the coupling time step i.e. the rate at which data between the CFD and CSM solvers was exchanged.

In LS-DYNA the rocks were modeled as rigid bodies with a density of 2.9 metric tons/m^3 corresponding to granite. The mass of rock 1 and the rock 2 was 4.1 kg (9.0 lb) and the mass of the rock 3 was 7.1 kg (15.6 lb). Three contact definitions were incorporated in the model: (i) among the moving rocks, (ii) between the moving rocks and the stationary rocks and (iii) between the moving rocks and the boundaries. It is sometimes advantageous in LS-DYNA to wrap solid bodies with null, massless shell elements to have more flexibility in defining the contact properties. One of advantages of such an approach in this case is the use of a non-zero thickness layer around the rocks that prevents them from coming into a full contact in STAR-CCM+. Using this method prevents morphed cells in a near contact zone from being squeezed to near zero volume and causing flow acceleration to unrealistically high velocities in crevices. The time step of calculations in the LS-DYNA explicit solver was set to 4.5×10^{-6} sec. Use of the explicit solver and such a small time step was needed to stabilize the contact forces between rocks colliding with other rocks or wall boundaries. A time step that is too large can cause excessive contact forces and abnormal behavior of the rocks. Once the STAR-CCM+ and LS-DYNA models were initialized, the coupling between them was activated.

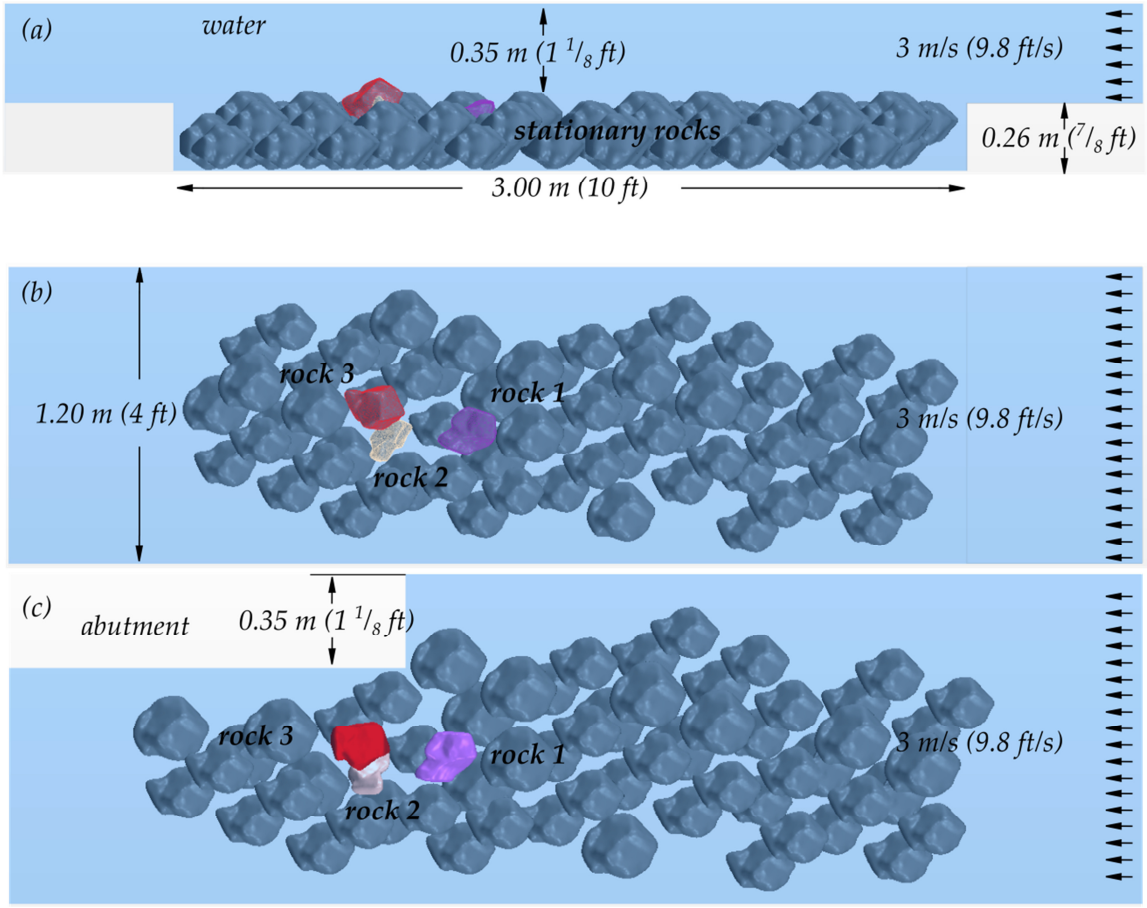

FIGURE 6 Geometry of the CFD model (a) layout 1, side view (b) layout 1, top view (c) layout 2, top view.

3.2 Results

Approximate values for critical velocity of the modeled rocks can be found by using Neill and Laursen equations *(10)*. Laursen's formula is given by equation 14:

$$V_{CL} = K_U y_2^{1/6} D_{50}^{1/3} \tag{14}$$

Where:

K_U is 6.19 for SI units or 11.7 for US customary units,

y_2 is the equilibrium scour flow depth (m or ft),

D_{50} is sediment size (m or ft).

For larger sediment sizes, above 0.03 m (0.1 ft), Neill's formula for critical velocity is defined by equation 15:

$$V_{CN} = 11.5\, K_U y_2^{1/6} D_{50}^{1/3} \tag{15}$$

Where:

K_U is 0.55217 for SI units or 1 for US customary units.

Taking y_2 = 0.35 m, D_{50} = 0.24 m, the critical velocities can be estimated around: V_{CN} = 3.31 m/s (10.8 ft/s) and V_{CL} = 3.23 m/s (10.6 ft/s). Based on that information, simulations were run with an inlet velocity of 2.0 m/s and increased by 0.5 m/s until a large displacement of a rock was observed. The results regarding the detection of motion of the rocks in specific runs are listed in Table 1. For both layout 1 and 2, at an inlet velocity of 2.0 m/s there was no significant motion of the rocks. For both layout 1 and 2 and an inlet velocity 2.5 m/s a local motion of rock 3 (the largest and most exposed to the flow) was

noticeable, but it was not moved out of its position. For layout 1 and an inlet velocity of 3.0 m/s, rock 3 was lifted out of position and moved into the downstream. Rock 2 also started to move locally. Snapshots from that simulation are shown in Figure 7. The fixed-in-place rocks were removed from the view for easier viewing of the moving rocks. A semi-transparent cross section through the domain showing the velocity distribution in the water is also shown in the figure. Snapshots of rocks from the simulation with layout 2 and inlet velocity of 3.0 m/s are shown in Figure 8.

TABLE 1 Motion of the Rocks in Two Analyzed Cases

inlet velocity	layout 1	layout 2
2.0 m/s	no motion	no motion
2.5 m/s	local motion of rock 3	local motion of rock 3
3.0 m/s	motion of rock 3 and local motion of rock 2	motion of rock 1 and 3

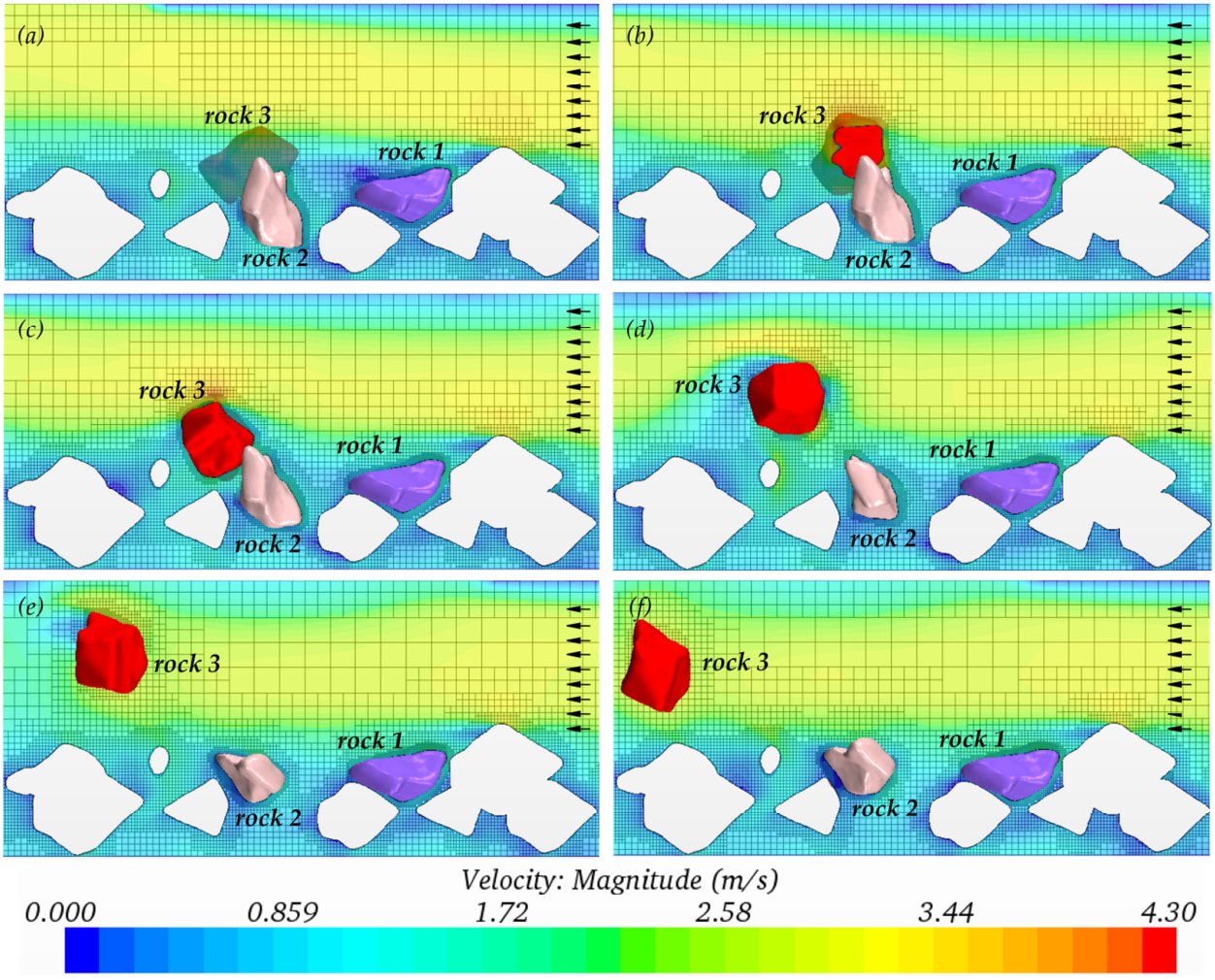

FIGURE 7 Snapshots from simulation for layout 1 and inlet velocity of 3.0 m/s.

4 SUMMARY AND FURTHER WORK

Procedures were developed to couple STAR-CCM+ CFD software and LS-DYNA CSM software to solve fluid structure interaction problems. The procedures include automated mapping and data exchange of the interface coupling conditions between the two software solvers. An automated recovery from mesh morphing errors that naturally arise when rocks approach contact with solid surfaces was successfully implemented. Two test cases were run and demonstrated that the analysis can be carried out with

reasonable use of TRACC cluster computational resources within a day for a domain residence time of about 2 seconds. The method is ready to be applied to the analysis of incipient motion of riprap at a variety of bridge structures, bed geometries, and flow conditions.

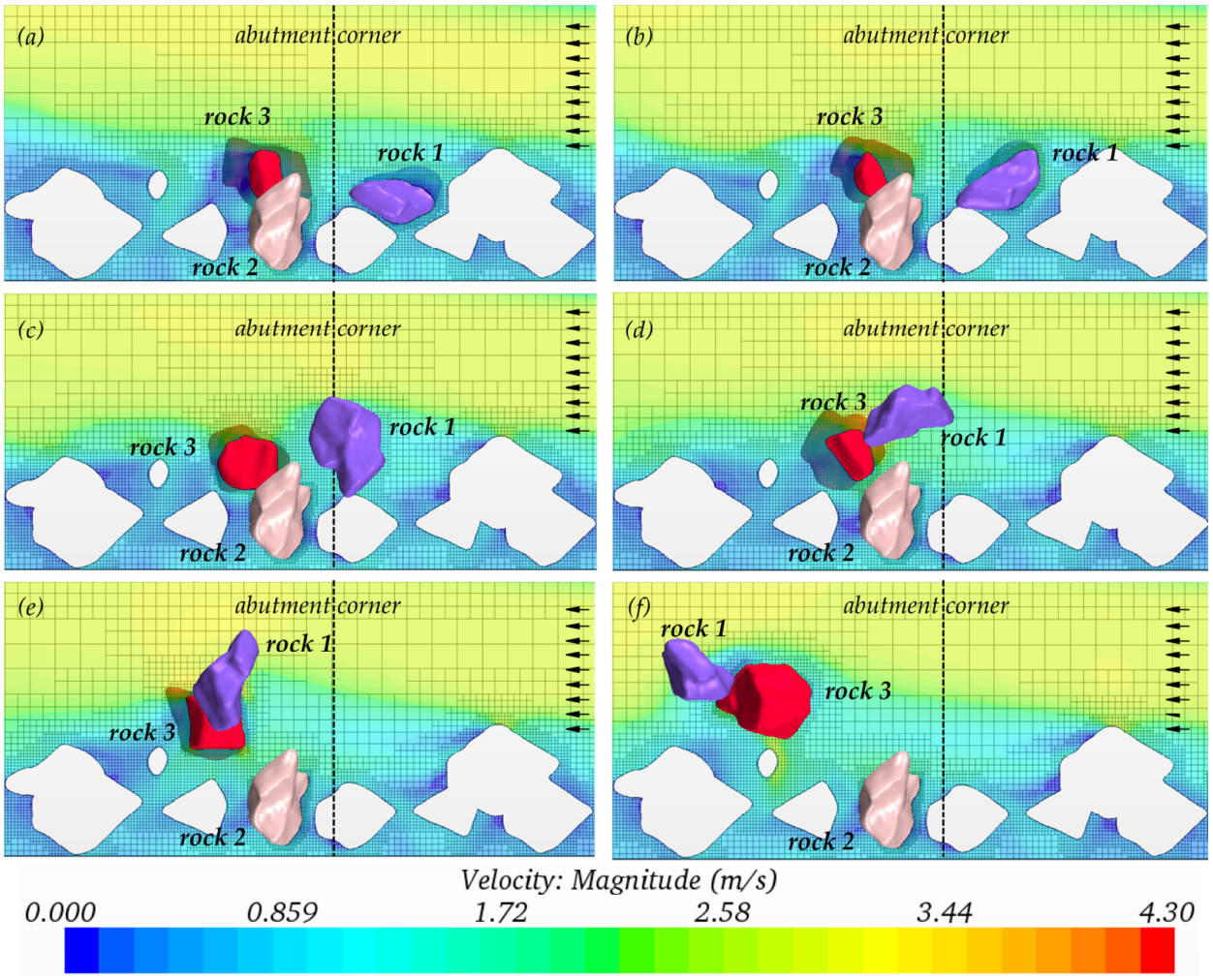

FIGURE 8 Snapshots from simulation for layout 2 and inlet velocity of 3.0 m/s.

ACKNOWLEDGEMENTS

The authors would like to acknowledge financial support and guidance by Dr. Kornel Kerenyi of TFHRC and thank Dr. Hubert Ley of Argonne National Laboratory, for the use of the high performance computers at Argonne's TRACC.

REFERENCES

(1) Lagasse P.F., Clopper P.E., Pagán-Ortiz J.E., Zevenbergen L.W., Arneson L.A., Schall J.D., Girard L.G., HEC-23 Bridge Scour and Stream Instability Countermeasures: Experience, Selection, and Design Guidance-Third Edition, Publication No. FHWA-NHI-09-111, U.S. Department of Transportation, 2009.

(2) Lagasse P.F., Clopper P.E., Zevenbergen L.W., Ruff J.F., NCHRP Report 568 Riprap Design Criteria, recommended Specifications, and Quality Control, Transportation Research Board, Washington, DC, 2006.

(3) J. Sterling Jones Hydraulics Research Laboratory, http://www.fhwa.dot.gov/research/tfhrc/labs/hydraulics/, Accessed: July 17, 2013.

(4) MeshLab, http://meshlab.sourceforge.net/ , Accessed: July 17, 2013.
(5) CD-Adapco User Guide STAR-CCM+ Version 8.02, 2013.
(6) Livermore Software Technology Corporation (LSTC), LS-DYNA® Keyword User's Manual Version 971, LSTC, 2007.
(7) Duarte F., Gormaz R., Natesan S., Arbitrary Lagrangian Eulerian method for Navier Stokes equations with moving boundaries, Methods Appl. Mech. Engrg., Vol.193, pp. 4819-4836, 2004.
(8) Hou G., Wang J., Layotn A., Numerical Methods for Fluid Structure Interaction – A Review, Commun. Comput. Phys., Vol. 12, No. 2, pp. 337-377, 2012.
(9) Livermore Software Technology Corporation (LSTC), Incompressible fluid solver in LS-DYNA, LSTC, 2013.
(10) Kerenyi K., Jones J., Stein S., Bottomless Culvert Scour Study: Phase II Laboratory Report, FHWA-HRT-07-026, U.S. Department of Transportation, 2007.